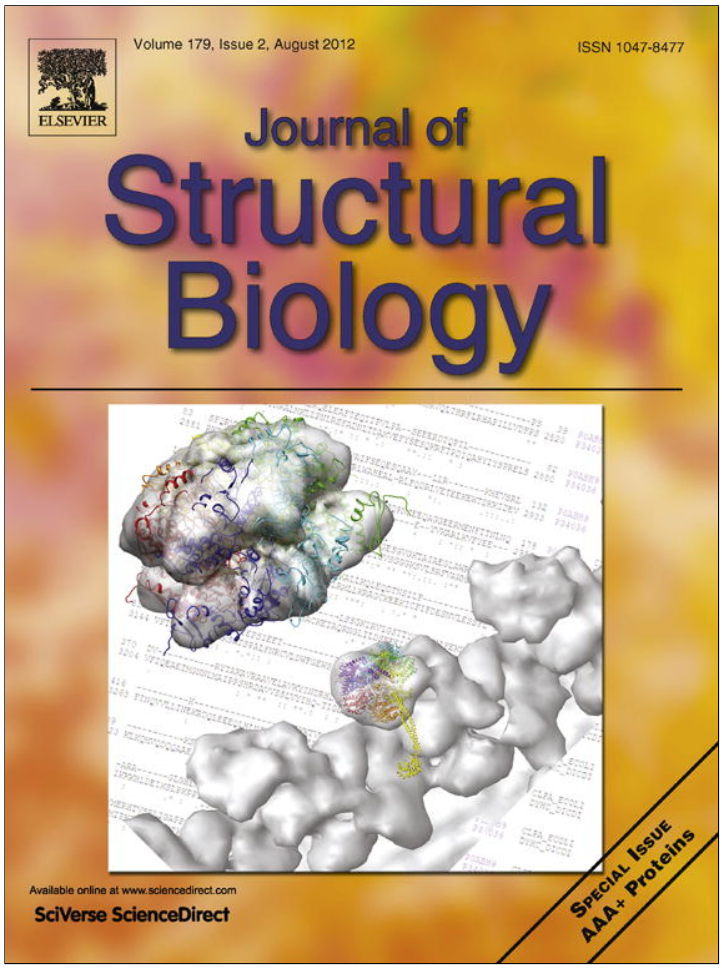

Journal of Structural Biology 179 (2012) 211–221

Contents lists available at SciVerse ScienceDirect

Journal of Structural Biology

journal homepage: www.elsevier.com/locate/yjsbi

Review

Novel structural and functional insights into the MoxR family of AAA+ ATPases

Keith S. Wong, Walid A. Houry *

Department of Biochemistry, University of Toronto, Toronto, Ontario, Canada M5S 1A8

ARTICLE INFO

Article history:
Available online 3 April 2012

Keywords:
MoxR
ATPases
Protein complex formation
Cofactor insertion
Stress response
RavA
von Willebrand factor A domain

ABSTRACT

The MoxR family of AAA+ ATPases is widespread among bacteria and archaea, although their cellular functions are not well characterized. Based on recent studies, MoxR ATPases are proposed to have chaperone-like function for the maturation of specific protein complexes or for the insertion of cofactors into proteins. MoxR proteins have been found to be important modulators of multiple stress response pathways in different organisms. For example, the respective MoxR proteins have been found to play important roles in the cell envelope stress response in *Rhizobium leguminosarum*, in the oxidative stress, acid stress, and heat stress responses in *Francisella tularensis*, in the acid stress and stringent responses in *Escherichia coli*, in viral tail formation in the crenarchaeal *Acidianus* two-tailed virus, and in the utilization of carbon monoxide as the sole carbon source by the Gram-negative chemolithoautotrophe *Oligotropha carboxidovorans*. Recent structural studies on the MoxR proteins from *E. coli* and *Cytophaga hutchinsonii* show the unique spatial arrangement of the αβα and all-α subdomains of the AAA+ domain in these proteins compared to the typical arrangement found in canonical AAA+ proteins such as HslU. The spatial organization of the subdomains in the AAA+ domain of MoxR proteins is similar to that found in the ATPase component of the magnesium chelatase complexes, possibly suggesting a similar mechanism of function. In this review, we provide an overview of the newly identified functions and the newly obtained structures of MoxR AAA+ ATPases.

1. Introduction to MoxR proteins

MoxR proteins constitute a family of AAA+ ATPases that is widespread among bacteria and archaea. In a previous bioinformatic analysis on the amino acid sequences of 596 complete AAA+ domains of MoxR proteins, we classified MoxR proteins into seven major subfamilies: MoxR Proper (MRP), TM0930, RavA, CbbQ/GvpN/NorQ (CGN), APE2220, PA2707, and YehL (Snider and Houry, 2006). A largely common feature of MoxR proteins is their co-occurrence with other proteins that carry the metal-binding von Willebrand factor A (VWA) domain. In most cases, these proteins are encoded in the genome immediately downstream of the gene for the respective AAA+ protein (Snider and Houry, 2006). Although the VWA domain is better characterized in eukaryotes than in prokaryotes, proteins having this domain are generally involved in mediating protein–protein interactions (Whittaker and Hynes, 2002; Springer, 2006). The key feature of the VWA domain is the presence of the non-contiguous MIDAS (Metal Ion-Dependent Adhesion Site) motif, which provides the binding site of a single divalent cation (usually Mg^{2+}) and is crucial for the domain's function (Whittaker and Hynes, 2002; Springer, 2006).

Despite the diversity and widespread occurrence of MoxR proteins, their functional characterization remains relatively limited to genetic studies, primarily, of members of the MRP and CGN subfamilies [see reference (Snider and Houry, 2006)]. Based on these studies, MoxR proteins are thought to have a chaperone-like activity, which is important for the maturation or assembly of specific protein complexes that are involved in dedicated metabolic pathways. MoxR proteins are also thought to be involved in cofactor insertion into specific proteins. For example, in *Paracoccus denitrificans*, MoxR (MRP subfamily) is important for the maturation of methanol dehydrogenase (MDH), although it has no effect on the biosynthesis of MDH itself, its cofactor pyrroloquinoline quinone (PQQ), or the associated electron acceptor cytochrome *c* (van Spanning et al., 1991). These findings also apply to *Methylobacterium extorquens* MoxR, in which case the protein is implicated in the insertion of Ca^{2+} into MDH during the enzyme's maturation process (Toyama et al., 1998). Similarly, NirQ and NorQ (CGN subfamily) have been shown experimentally to be important for the activation of the nitric oxide reductase enzyme involved in denitrification, but without any effects on the expression of the denitrification proteins (Jungst and Zumft, 1992; Arai et al., 1999). This has been illustrated for NirQ/NorQ in *Pseudomonas aeruginosa*, *Pseudomonas stutzeri*, *P. denitrificans*, and *Rhodobacter*

* Corresponding author. Address: 1 King's College Circle, Medical Sciences Building, Department of Biochemistry, University of Toronto, Toronto, Ontario, Canada M5S 1A8. Fax: +1 416 978 8548.
E-mail address: walid.houry@utoronto.ca (W.A. Houry).

1047-8477/$ - see front matter © 2012 Elsevier Inc. All rights reserved.
http://dx.doi.org/10.1016/j.jsb.2012.03.010

sphaeroides 2.4.3 (Jungst and Zumft, 1992; de Boer et al., 1996; Bartnikas et al., 1997; Arai et al., 1999).

In this review, we will provide an update on our current knowledge of the MoxR proteins with the most recent experimental characterization of known and newly identified members of this diverse family of AAA+ ATPases. Importantly, the recently solved crystal structures of the *Escherichia coli* RavA and *Cytophaga hutchinsonii* CHU_0153, which belong to the RavA and MRP subfamilies, respectively, provide detailed structural insights into MoxR proteins in general, and in turn allows for the first identification of distinctive structural features that are potentially unique to MoxR family proteins.

2. Recent functional characterization of MoxR proteins

In the first part of this review, we will focus our discussion on the most recent functional characterization of both known and newly identified MoxR proteins. The newly characterized functions of these proteins are summarized in Table 1.

2.1. Roles of MRP in stress tolerance, cell development, and bacterial pathogenesis

2.1.1. RL3499 from Rhizobium leguminosarum

RL3499 encodes a newly identified MoxR protein of the MRP subfamily in *R. leguminosarum* Biovar *viciae* (Vanderlinde et al., 2011), a soil-dwelling Gram-negative bacterium that forms a symbiotic relationship with leguminous plants (Newton, 2000; Oldroyd and Downie, 2008). Using a general screen utilizing 1750 individual transposants, Vanderlinde and coworkers (Vanderlinde et al., 2011) identified RL3499, located in the gene cluster RL3499–RL3502, as being essential for *R. leguminosarum* growth in rich medium. The gene cluster has the expected organization of MRP subfamily members (Snider and Houry, 2006) (Fig. 1A): RL3499 is followed immediately downstream by RL3500, which encodes a protein that contains a domain of unknown function, DUF58; RL3500 is in turn followed downstream by RL3501, which encodes a 937-residues-long protein with a predicted N-terminal double-transmembrane domain, a VWA domain in the middle, and a C-terminal class-I glutamine amidotransferase (GATase) domain; RL3502 is a putative transmembrane protein. The gene cluster RL3499–RL3502 was found to be important for growth of *R. leguminosarum* in the presence of reagents such as SDS, erythromycin (a hydrophobic antibiotic), and polymyxin B, which weakens the cell envelope (Vanderlinde et al., 2011). The gene cluster was also found to be important for growth at alkaline pH (Vanderlinde et al., 2011), a condition that has been reported to reduce the rate of peptidoglycan cross-linking in *Bacillus* sp. C-125 (Aono and Sanada, 1994). RL3499–RL3502 was required for growth in rich or minimal media in the presence of glycine or peptides, which are known to increase cell envelope permeability (Hammes et al., 1973; Li et al., 2009). Accordingly, Ca^{2+} and Mg^{2+} that stabilize cell envelope integrity (Vaara, 1992; Dominguez, 2004) can reverse the growth defects of mutants lacking RL3499–RL3502 to various degrees, depending on the exact growth conditions (Vanderlinde et al., 2011). Importantly, RL3499–RL3502 was found to be crucial for maintaining normal cell morphology, as well as, symbiosis with the host pea plant *Pisum sativum* (Vanderlinde et al., 2011). These phenotypes thus highlight a major role of RL3499 in maintaining cell envelope integrity, which in turn is important for the symbiosis between *R. leguminosarum* and the pea plant (Table 1). However, the protein target of RL3499 activity is not known.

2.1.2. FTL_0200 from Francisella tularensis

Another recently characterized MRP protein is FTL_0200 from *F. tularensis* (Dieppedale et al., 2011), a Gram-negative pathogen that causes tularaemia in humans and many animal species (Santic et al., 2010). The *FTL_0200* gene is located the furthest upstream in the gene cluster *FTL_0200–FTL_0206* (Dieppedale et al., 2011), which has the expected gene organization for MRP subfamily members (Snider and Houry, 2006) (Fig. 1B). *FTL_0200* is followed immediately downstream by *FTL_0201*, which contains sequential motifs for both VWA and DUF58 domains (Dieppedale et al., 2011). Two additional VWA proteins are encoded by *FTL_0203* and *FTL_0204*, respectively, with *FTL_0204* also carrying motifs for the Tetratricopeptide Repeat (TPR) domain. *FTL_0205*, which encodes a second TPR protein, follows immediately downstream. The last gene in this cluster is *FTL_0206* (Dieppedale et al., 2011), which encodes a homolog of the an oxygen tolerance-associated protein BatD from the obligate anaerobe *Bacteroides fragilis* (Tang et al., 1999). Promoter region analysis and gene expression data suggest that the expression of the *FTL_0200–FTL_0206* gene cluster is likely inducible by the heat shock-associated transcriptional regulator σ^{32} (Dieppedale et al., 2011).

Function wise, although insertional mutations to *FTL_0200* (MRP gene), *FTL_0205* (TPR gene) and *FTL_0206* show no growth defects in liquid media, all three mutants show significantly impaired ability to infect THP1 (human acute monocytic leukemia cell line) and J774 (murine macrophage cell line) cells compared to wild type (Dieppedale et al., 2011). The three mutants also exhibit reduced infectivity of all three insertional mutants in the mouse model (Dieppedale et al., 2011). Further analysis using a *FTL_0200* deletion mutant shows that the MoxR protein is important for tolerance to oxidative stress, acid stress, heat stress, and the

Table 1
Recent functional characterization of MoxR proteins.

Protein	Organism	MoxR subfamily classification	Cellular/molecular functions	Reference
RL3499	*Rhizobium leguminosarum* Biovar *viciae*	MRP	• Cell envelope development • Cell morphology • Stress tolerance • Bacterium-host symbiosis	(Vanderlinde et al., 2011)
FTL_0200	*Francisella tularensis*	MRP	• Acid & oxidative stress resistance • Bacterial pathogenesis	(Dieppedale et al., 2011)
RavA	*Escherichia coli* K-12	RavA	• Prevents inhibition of the inducible lysine decarboxylase LdcI • Role in acid stress & stringent responses	(El Bakkouri et al., 2010)
p618	*Acidianus* two-tailed virus	RavA	• DNA binding • Possible role in extracellular viral tail development	(Scheele et al., 2011)
CoxD	*Oligotropha carboxidovorans* OM5	APE2220	• Partial unfolding of apo-CO dehydrogenase • CO dehydrogenase maturation	(Pelzmann et al., 2009)

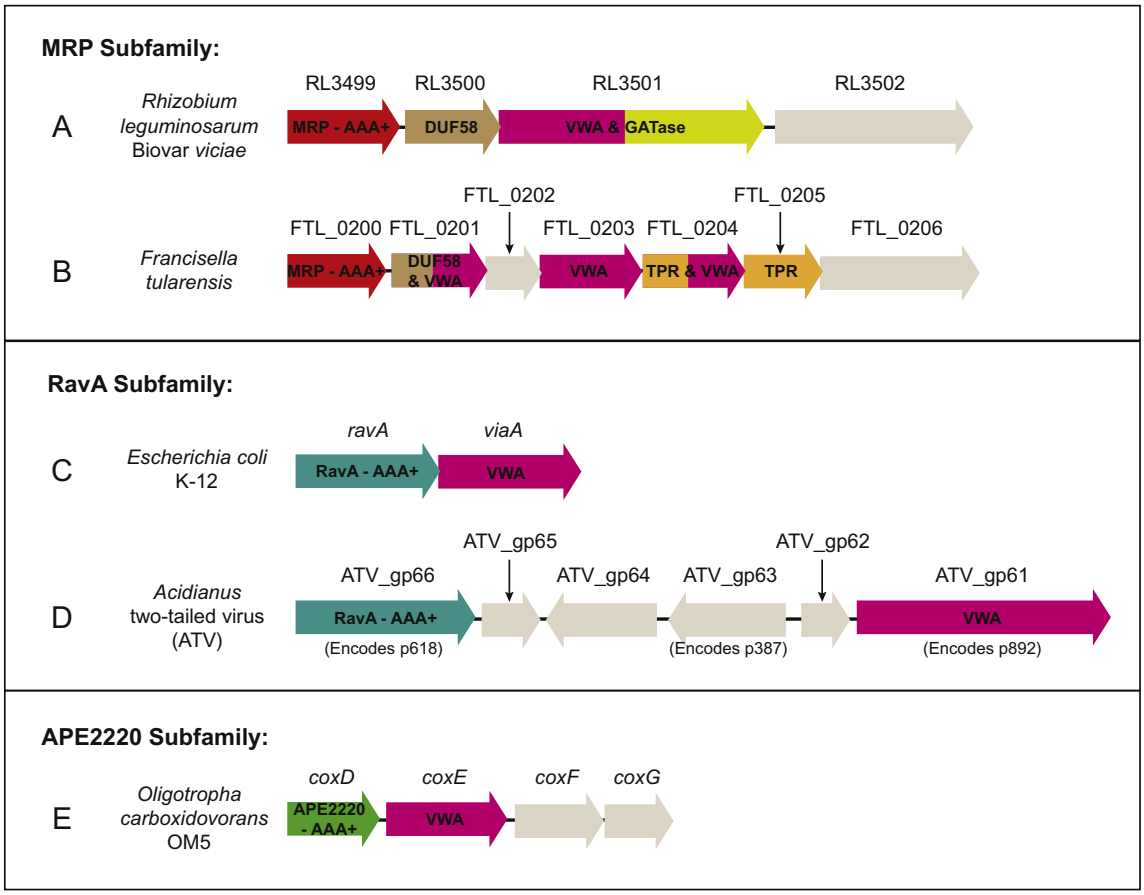

Fig.1. Gene organization of different MoxR-containing gene clusters. Shown are schematics for the MoxR-containing gene clusters found in (A) *R. leguminosarum* Biovar *viciae*, (B) *F. tularensis*, (C) *E. coli* K-12, (D) *Acidianus* two-tailed virus (ATV), and (E) *O. carboxidovorans* OM5. Gene clusters containing MoxR proteins from the same subfamily are grouped together as shown. All genes encoding for the different MoxR proteins, VWA proteins, and other proteins that are characteristic of the different MoxR subfamilies are colored and their key domains/motifs are identified. All other genes are colored in gray. For each gene cluster, genes are oriented relative to their respective MoxR-encoding gene.

presence of protein denaturants such as ethanol and SDS (Dieppedale et al., 2011). The combined data thus strongly suggest a role for FTL_0200 in multiple stress tolerance pathways, as well as, in *Francisella* pathogenesis (Table 1).

Taken together, both RL3499 and FTL_0200 provide the first examples that MRP proteins are also associated with a variety of important cellular functions other than their traditional role in metabolism. These range from stress tolerance, cell morphology and development, bacterium-host interaction, to pathogenesis.

2.2. Roles of RavA in acid stress, stringent response, and viral tail formation

2.2.1. RavA from E. coli

RavA from *E. coli* K-12 is the first member of the RavA subfamily that has been extensively characterized (Snider et al., 2006; El Bakkouri et al., 2010). Its corresponding VWA protein is known as ViaA (Snider et al., 2006; Snider and Houry, 2006). Like other members of the RavA subfamily, the *ravA* gene is encoded immediately upstream of the *viaA* gene in the same operon (Snider et al., 2006; Snider and Houry, 2006) (Fig. 1C), which is inducible by the alternative transcriptional regulator σ^S in aerobically grown cells during stationary phase (Snider et al., 2006). In the presence of ATP or other nucleotides, RavA forms a hexamer via its AAA+ domain (see below) (Snider et al., 2006; El Bakkouri et al., 2010). The ATPase activity of RavA is optimal at neutral pH and is comparable to other well-characterized AAA+ ATPases such as HslU, NtrC, and Lon protease (Snider et al., 2006). The interaction of RavA with ViaA has been observed *in vitro*, which increases RavA's ATPase activity by about 2-fold (Snider et al., 2006). Importantly, RavA interacts strongly and specifically with the inducible lysine decarboxylase LdcI (Snider et al., 2006; El Bakkouri et al., 2010), which is an important acid stress response enzyme (Kanjee et al., 2011). This interaction, which requires the LARA (LdcI associating domain of RavA) domain of RavA (El Bakkouri et al., 2010), results in a large cage-like structure consisting of two LdcI decamers and up to five RavA hexamers (Snider et al., 2006) (further discussed below). The RavA-LdcI interaction results in a 1.4-fold increase in RavA's ATPase activity (Snider et al., 2006).

Although the function of *E. coli* RavA is not well established, RavA has been shown to de-inhibit LdcI activity by preventing the binding of a potent LdcI inhibitor, the stringent response alarmone, guanosine 3′, 5′-bis(diphosphate) (ppGpp) (Kanjee et al., 2011), both *in vitro* and *in vivo* (El Bakkouri et al., 2010) (Table 1). The alarmone ppGpp is a bacterial signaling molecule that mediates the bacterial stringent response, which is elicited as a consequence of amino acid starvation or other nutritional stresses resulting in changes to the transcriptional profile of cells; this causes a switch in growth phase from exponential to stationary phase (Cashel et al., 1996; Nystrom, 2004). Under these conditions, there is an overall down-regulation of processes involved in cell proliferation including DNA replication, rRNA and tRNA transcription, production of ribosomes, cell membrane synthesis, and general biomolecular synthesis, and a concomitant up-regulation of

genes involved in stationary phase, stress survival, amino acid biosynthesis, and nutritional scavenging. The stringent response effects are primarily mediated by guanosine tetraphosphate ppGpp and guanosine pentaphosphate pppGpp (guanosine 3′-diphosphate, 5′-triphosphate), collectively known as (p)ppGpp. The *E. coli* RNA polymerase (RNAP) is a main target of (p)ppGpp binding, which results in the 'reprogramming' of the polymerase and change in the transcriptional profile of the cell. However, there are other protein targets of (p)ppGpp including LdcI.

Thus, the RavA-LdcI interaction has been proposed to be a regulatory mechanism by which the cell can switch LdcI activity between the LdcI-mediated acid stress response, which consumes lysine in the process, and the conservation of amino acids during stringent response (El Bakkouri et al., 2010; Kanjee et al., 2011). It should be noted that the exact role of ViaA in this process is not yet clear.

2.2.2. p618 from the crenarchaeal Acidianus two-tailed virus (ATV)

A novel member of the RavA subfamily that was recently characterized is p618 from the crenarchaeal *Acidianus* two-tailed virus (ATV) (Scheele et al., 2011). Its primary sequence shares a 21% identity and 42% similarity with *E. coli* RavA. Structurally, the hexameric form of the Walker B mutant of p618 shows a close resemblance to that of wild type *E. coli* RavA in the presence of nucleotides. Biochemically, the K_m value for the ATPase activity of p618 (~0.55 mM) (Scheele et al., 2011) is very similar to that of *E. coli* RavA (~0.79 mM) (Snider et al., 2006). However, unlike *E. coli* RavA, the ATPase activity of p618 is optimal at high temperature, due to the fact that ATV's host, the hyperthermophile *Acidianus convivator*, dwells in an acidic environment with temperatures ranging from 85 to 93 °C (Scheele et al., 2011).

The equivalent of the ViaA protein for p618 is p892. Unlike for other members of the RavA subfamily, the p892-encoding gene, ATV_gp61, does not immediately follow downstream of the p618-encoding gene, ATV_gp66. Instead, they are separated by four genes: ATV_gp62, ATV_gp63, ATV_gp64 and ATV_gp65 (Fig. 1D) (Prangishvili et al., 2006). Importantly, this is the first report of a RavA-containing gene cluster not having the typical gene organization of the RavA subfamily. Strong interaction between p618 and p892 has been observed *in vitro*, which requires the AAA+ domain of p618 and is enhanced by the presence of ATP and Mg^{2+} (Scheele et al., 2011). Similar to *E. coli* ViaA, the presence of p892 also increases the ATPase activity of p618 (Scheele et al., 2011). Unlike *E. coli* ViaA, however, p892 forms tetramers and hexamers *in vitro* and binds linear, double-stranded DNA in a non-specific manner *in vitro* (Scheele et al., 2011) – a property not observed in its *E. coli* counterpart [(Snider et al., 2006) and KW & WAH, unpublished data]. Interestingly, while p618 alone does not show any affinity for DNA, its interaction with p892 completely inhibits the VWA protein from binding to DNA (Scheele et al., 2011). Aside from p892, three additional ATV proteins, p387 (ATV_gp63, Fig. 1D), p653, and p800, were found to interact physically with p618 (Scheele et al., 2011). p387 has 61.5% sequence identity to p653, and they both exhibit affinity for linear, double-stranded DNA in a non-specific manner (Scheele et al., 2011). On the other hand, p800 is known to form filaments spontaneously via self-aggregation and has been implicated in viral tail development (Prangishvili et al., 2006). Taken together, the interactions of p618 with DNA-binding proteins and a putative viral tail structural protein suggest a possible role of this RavA subfamily member protein in the viral tail formation of ATV (Scheele et al., 2011) (Table 1). Given that the two viral tails are formed after the ATV virion has extruded from the host cell, the ATP required for p618 activity is proposed to be available from a pool of encapsulated cellular ATP within the ATV virion that it acquires from the host cell during the extrusion process (Scheele et al., 2011).

2.3. Newly identified role of APE2220 in protein maturation

2.3.1. CoxD from Oligotropha carboxidovorans

The Gram-negative chemolithoautotroph (an organism that obtains energy from inorganic compounds and carbon from CO_2) *O. carboxidovorans* OM5 requires the carbon monoxide (CO) dehydrogenase complex for utilizing CO as a sole source of energy. The complex exists as a dimer-of-trimers, with each trimer consisting of the subunits CoxL, CoxM and CoxS (Dobbek et al., 1999). The catalytic site for the oxidation of CO, located in the CoxL subunit of the complex, contains a unique [$CuSMoO_2$] cluster (Meyer et al., 2000). The proper assembly of this cluster into CoxL requires the AAA+ ATPase CoxD, which belongs to the APE2220 subfamily (Pelzmann et al., 2009). Notably, this is the first APE2220 protein to be assigned a definitive biological function (Snider and Houry, 2006). CoxD is encoded in the gene cluster *coxDEFG* (Fig. 1E) located downstream of *coxMSL* that encodes the CO dehydrogenase subunits (Pelzmann et al., 2009). The *coxE* gene, which immediately follows *coxD* (Fig. 1E), is predicted to encode a VWA protein (Fuhrmann et al., 2003) and is likely to be the corresponding VWA protein partner for CoxD.

CoxD can utilize both ATP and GTP (Pelzmann et al., 2009), and was found to be essential for the activity of CO dehydrogenase, as disruption of *coxD* inhibits *O. carboxidovorans* from utilizing CO as a sole energy source although there is no effect on the expression of CO dehydrogenase subunits (Pelzmann et al., 2009). CO dehydrogenase purified from the *coxD* insertional mutant was found to be inactive due to the lack of a properly assembled [$CuSMoO_2$] cluster, while the rest of the electron transfer relay, consisting of two [2Fe–2S] clusters found in the CoxS and a redox-active FAD in CoxM (Meyer et al., 2000), remained intact (Pelzmann et al., 2009). Importantly, the enzymatic activity of apo-CO dehydrogenase isolated from the *coxD* mutant can be restored by a step-wise reconstitution of the [$CuSMoO_2$] cluster *in vitro*, which first involves the resulfuration of the MoO_3 moiety found in the apo-enzyme, followed by the introduction of copper (Pelzmann et al., 2009). Based on these data, the role of CoxD has been proposed to be for the partial unfolding of CoxL to allow for the step-wise assembly of the [$CuSMoO_2$] cluster (Table 1), although no *in vitro* data is available for verifying this claim due to the reported difficulty in isolating soluble CoxD in its functional form (Pelzmann et al., 2009). Given the apparent association of CoxD with the inner membrane of *O. carboxidovorans* and the fact that CO dehydrogenase is cytoplasmic, the CoxD-dependent assembly of the [$CuSMoO_2$] cluster is proposed to occur on the cytoplasmic side of inner membrane (Pelzmann et al., 2009).

3. Structural characterization of MoxR proteins

The primary focus of this section will be placed on the recently solved crystal structures of the *E. coli* RavA (PDB ID 3NBX) (El Bakkouri et al., 2010) and the MoxR (MRP) AAA+ ATPase, CHU_0153, from *C. hutchinsonii* (PDB ID 2R44, Joint Center for Structural Genomics), both of which possess structural features that are potentially unique to MoxR family proteins in general. We will first discuss the structural aspects of the AAA+ domain of the MoxR proteins and then provide a detailed discussion of the structure of the *E. coli* RavA–LdcI complex.

3.1. The unique subdomain arrangement in the AAA+ domain of MoxR proteins

Examination of the AAA+ domains of *E. coli* RavA (Fig. 2A), *C. hutchinsonii* CHU_0153 (Fig. 2B), and the closely related magnesium chelatase AAA+ subunit BchI from *Rhodobacter capsulatus*

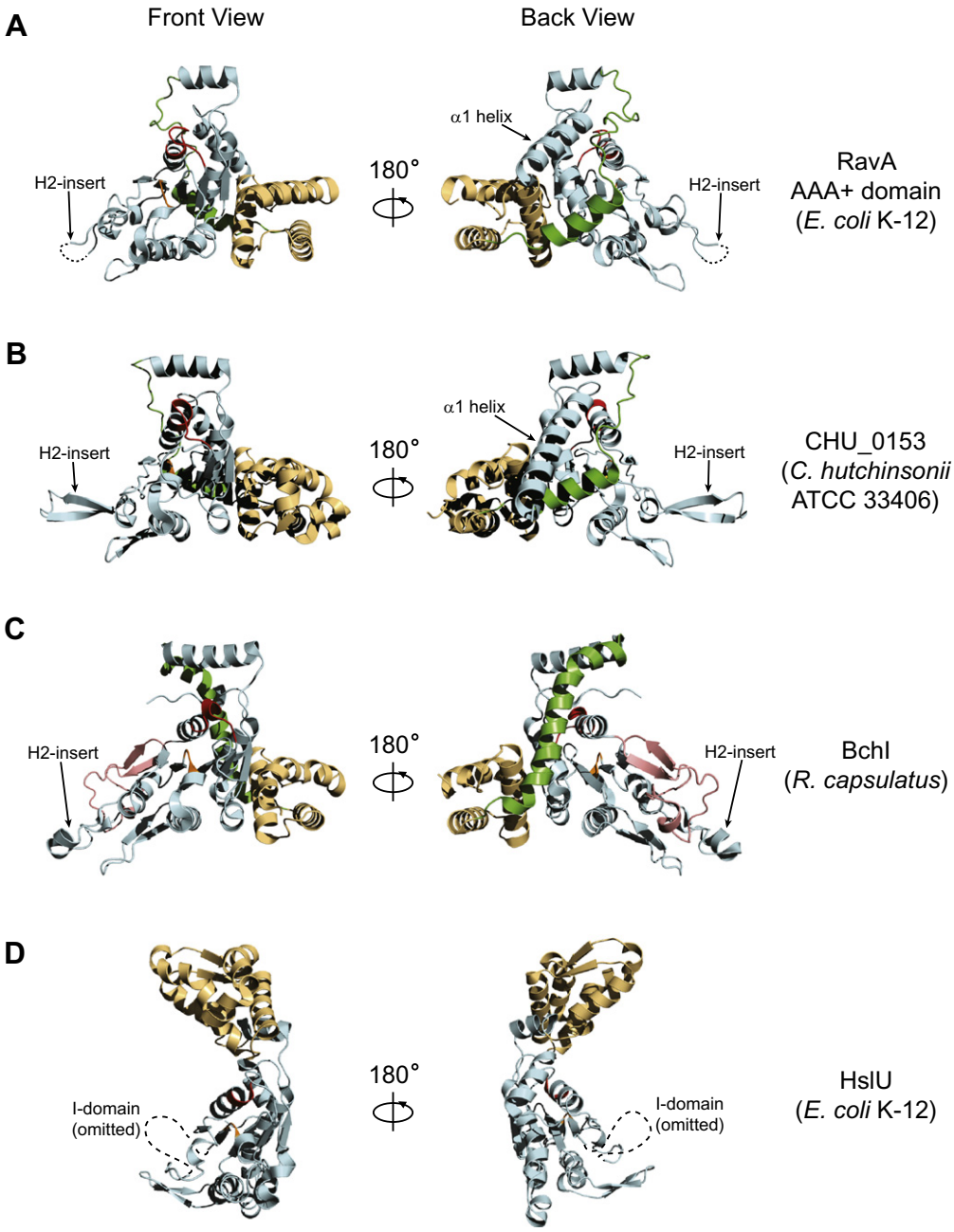

Fig.2. Structures of the AAA+ domain of MoxR proteins. Shown are the crystal structures of (A) the AAA + domain of RavA from *E. coli* K-12 (PDB ID 3NBX), (B) CHU_153 (YP_676785.1) from *C. hutchinsonii* ATCC 33406 (PDB ID 2R44), (C) BchI from *R. capsulatus* (PDB ID 1G8P), and (D) HslU from *E. coli* K-12 (PDB ID 1DO0). The αβα subdomains are colored in light blue and the all-α subdomains in gold. Linker regions of RavA, CHU_153, and BchI are colored green. The Walker A and Walker B motifs are highlighted in red and orange, respectively. The α1-β2-β-hairpin unique to BchI (Snider et al., 2008) is highlighted in pink. Helix-2 inserts (H2-insert) and α1 helices are indicated as shown. The dotted line in (A) indicates the unstructured region that is not resolved in the X-ray crystal structure of RavA. Both the front (with nucleotide binding site facing the reader) and back views of the AAA+ domains are shown for all four proteins. For simplicity, the bound nucleotides in RavA and HslU, as well as, the I-domain of HslU, have been omitted. The structures were generated using PYMOL.

(Fig. 2C) revealed important structural characteristics that are in common. These three proteins belong to the Helix-2 insert clade, which includes both the MoxR family and the magnesium chelatase family (Iyer et al., 2004). The most striking structural characteristic is the unique spatial arrangement of the αβα and all-α subdomains of the AAA+ domain, compared to the typical configuration found in other AAA+ proteins. The αβα subdomain contains the canonical Walker A and Walker B motifs responsible for nucleotide binding and hydrolysis, Sensor 1 that senses nucleotide binding/hydrolysis, and the Arg finger that interacts with nucleotide bound by the neighboring subunit (Snider et al., 2008). The all-α subdomain contains the Sensor 2 motif that has a conserved Arg, which interacts with the γ-phosphate of the bound ATP (Snider et al., 2008). Using *E. coli* HslU as an example of a canonical AAA+ ATPase (Fig. 2D), it can be noted that while the all-α subdomain is usually positioned on 'top' of the αβα subdomain, the all-α subdomain in RavA, CHU_0153, and BchI is rearranged to the 'side' of the αβα subdomain. This unique spatial arrangement is made possible by the presence of a linker region (colored in green in Fig. 2A–C) that spans along the 'back' of the αβα subdomain (back view in Fig. 2A–C). The linker region has been previously shown to be a unique characteristic among AAA+ ATPases belonging to the Helix-2 insert clade (Iyer et al., 2004).

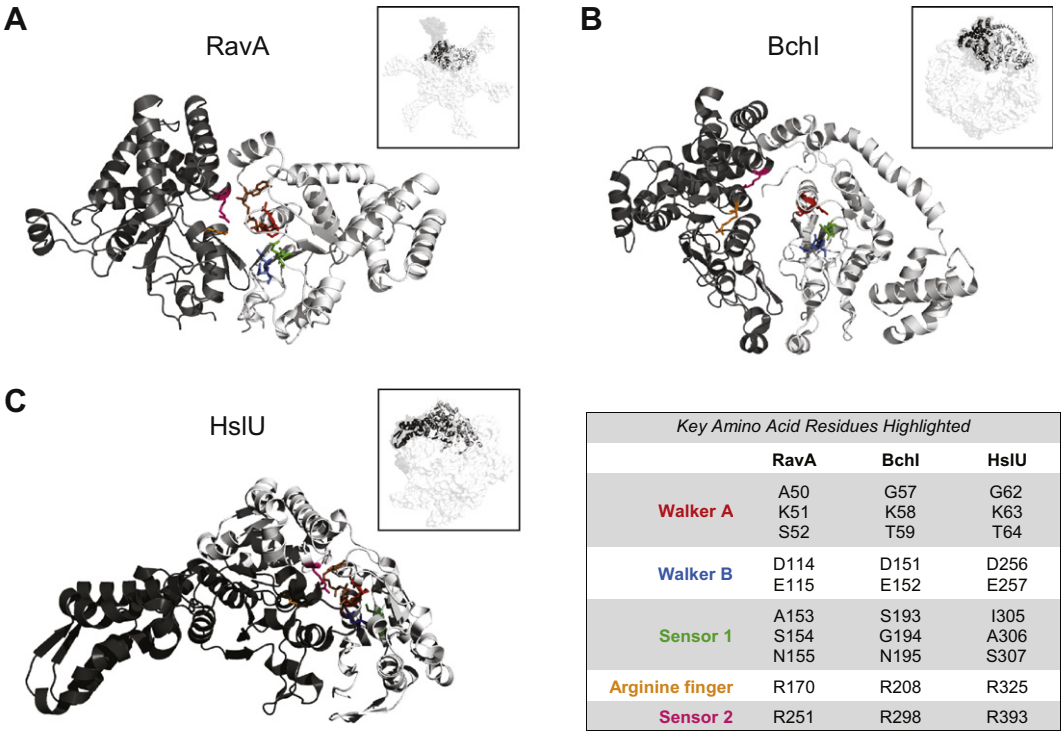

Fig.3. Nucleotide binding site in MoxR proteins. Shown are two adjacent AAA+ domains with the respective nucleotide binding site between the two subunits for (A) *E. coli* RavA, (B) *R. capsulatus* BchI, and (C) *E. coli* HslU (PDB ID 1DO0). One subunit is colored dark gray, while the other subunit is colored white. The important functional motifs of the nucleotide binding sites have their key amino acid residues displayed in stick format, and are colored as follows: red, Walker A; blue, Walker B; green, Sensor 1; orange, Arginine finger; magenta, Sensor 2. The key residues highlighted are as given in the chart at the lower-right corner. All bound nucleotides are shown in stick format and colored in brown. BchI has no bound nucleotide. For simplicity, only the AAA+ domains are shown and other domains have been removed. The insets show the orientation of the two subunits (shown in ribbon format) relative to the full length hexameric complex (with the accessible surfaces shown).

The X-ray structures of *E. coli* RavA, *C. hutchinsonii* CHU_0153, and *R. capsulatus* BchI are those of monomers and not hexamers. However, 3D electron microscopy (EM) reconstructions are available for RavA (El Bakkouri et al., 2010) and BchI hexamers (Lundqvist et al., 2010). By fitting the monomer X-ray structure into the hexamer EM maps, it can be deduced that despite the unusual subdomain arrangement, the ATP-binding pocket at each dimer interface in RavA and BchI (and presumably CHU_0153) is expected to be similar to the one found in a canonical AAA+ domain such as that of *E. coli* HslU, whose X-ray structure was solved as a hexamer (Bochtler et al., 2000; Wang et al., 2001). As shown in Fig. 3, the five essential functional motifs (Walker A, Walker B, Sensor 1, Arginine finger, and Sensor 2) are all conserved in their spatial coordination relative to the nucleotide-binding pocket. The only alteration to the pocket as a result of the different subdomain arrangement is in Sensor 2. Specifically, with the canonical subdomain arrangement of HslU, Sensor 2 is contributed by the same monomeric subunit as Walker A, Walker B and Sensor 1 (Fig. 3C), while in the alternative subdomain arrangement of RavA and BchI, it originates from the adjacent monomeric subunit instead (i.e. the same subunit that contributes the Arginine finger) (Fig. 3A and B). The functional significance of having an alternative subdomain arrangement in RavA, CHU_0153, and BchI is not known and warrants further investigation. It should be noted that, in BchI, the arginine side chain of Sensor 2 and the Arginine finger both point away from the nucleotide-binding pocket in the X-ray structure (Fig. 3B), which might reflect a different nucleotide state or may simply be an artifact (Fodje et al., 2001).

3.2. Structural features unique to the AAA+ domain of MoxR proteins

The overall structural layouts of the AAA+ domains of RavA and CHU_0153 highly resemble that of BchI (Fig. 2). Nevertheless, a closer examination reveals key differences that distinguish RavA and CHU_0153 as members of a different protein family from BchI. For example, the linker region in BchI is largely helical in structure with two minor kinks at both ends, which gives it a slightly S-shaped conformation (Fig. 2C). However, in both RavA and CHU_0153, only a small helical segment is present in the C-terminal half of the linker, while the N-terminal half forms flexible loops (Fig. 2A and B). The orientation of the helical segment in the linker is also different. In BchI, the helical segment runs along the back of the αβα subdomain from top to the bottom before reaching the all-α subdomain (Fig. 2C), while in RavA and CHU_0153, it lies at a small angle to the base of the αβα subdomain, with the C-terminal end pointing downwards leading into the all-α subdomain (Fig. 2A and B). The primary reason for this difference is due to physical constraint, as both RavA and CHU_0153 have a long α1 helix at the N-terminus (back view in Fig. 2A and B) that occupies the same space as the helical linker region in BchI (back view in Fig. 2C). Note that the length of the linker region for RavA (33 residues), CHU_0153 (29 residues), and BchI (32 residues) are very similar (Fig. 4). Based on multiple sequence alignment of the three AAA+ domains (Fig. 4), it is interesting to note that although their respective linker regions are well aligned in the C-terminal half, where all three are helical in structure, the N-terminal half is not. This is likely to contribute to differences in tertiary structure.

Another structural difference between RavA/CHU_0153 and BchI lies in the H2-insert and its immediate surroundings. As observed in RavA and CHU_0153, the H2-insert adopts a simple unstructured loop (Fig. 2A) or β-hairpin motif (Fig. 2B), respectively. However in BchI, the H2-insert adopts a strand-loop-helix-loop-strand motif. There is also an α1-β2-β-hairpin in the vicinity (Fig. 2C, highlighted in pink and Fig. 4, highlighted in gray), which is unique to magnesium chelatases (Snider et al., 2008) and is ab-

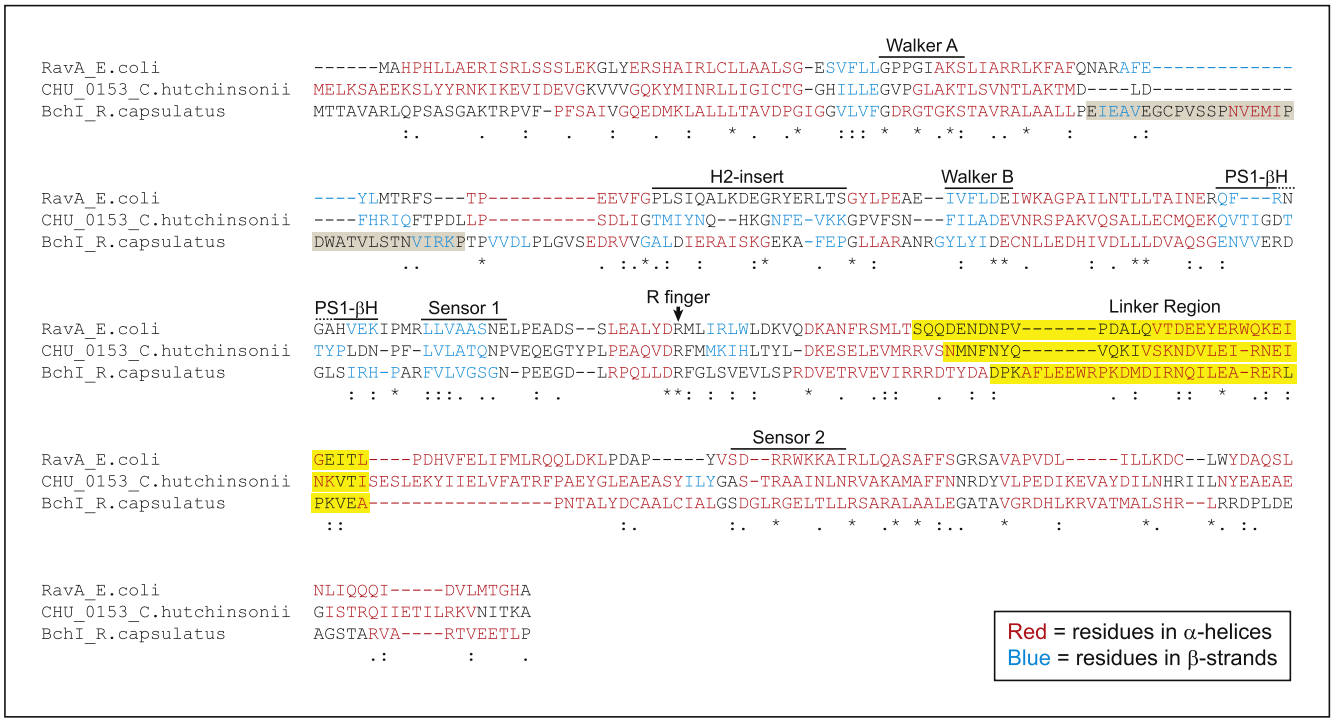

Fig.4. Multiple sequence alignment of the AAA+ domain of RavA, CHU_153, and BchI. The multiple sequence alignment was generated using MUSCLE (Edgar, 2004). All information on secondary structures is derived from the crystal structures of the three proteins. Residues colored in red are found in α-helices, and those in blue are found in β-strands. The linker region is highlighted in yellow. The α1-β2-β-hairpin unique to magnesium chelatases (Snider et al., 2008) is highlighted in gray. Important sequence motifs of the AAA + domain, the Helix-2 insert (H-2 insert), and the Pre-sensor 1 β-hairpin (PS1-βH) are all shown as indicated. In the alignment, '∗' denotes identical amino acid residues, ':' denotes highly similar amino acid residues and '.' denotes similar amino acids.

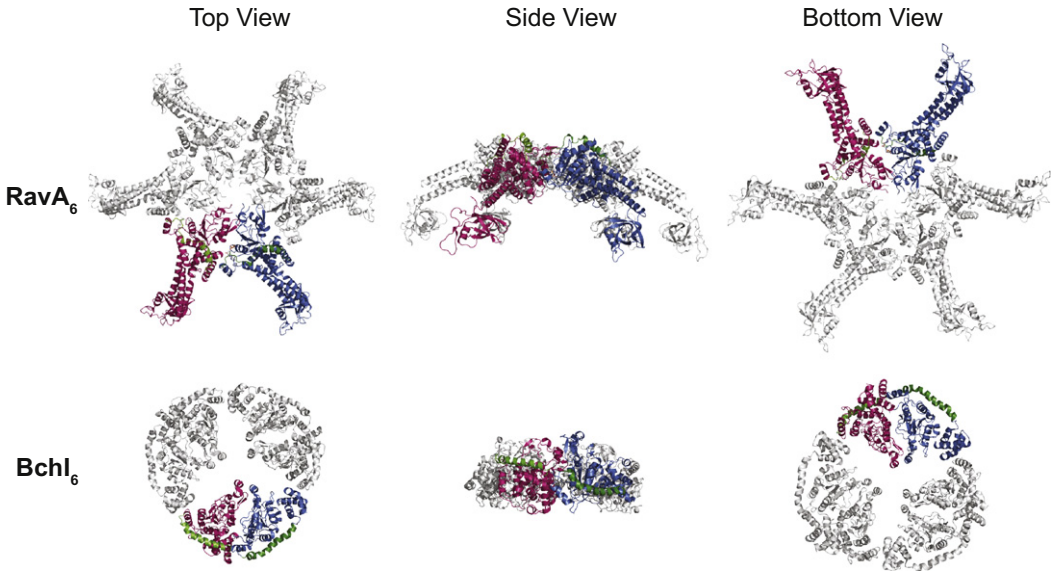

Fig.5. The RavA and BchI hexameric assembly. Shown are the top, side, and bottom views of the RavA hexamer (top row) and BchI hexamer (bottom row). For the RavA hexamer, two consecutive subunits are shown in red and blue. For BchI, which forms a trimer-of-dimers, two subunits that belong to the same dimer are highlighted in red and blue. The linker regions are highlighted in green. Both RavA and BchI hexamers were obtained by modeling the crystal structure of the monomer onto the respective EM structure of the hexamer in the ADP-bound state (El Bakkouri et al., 2010; Lundqvist et al., 2010).

sent in both RavA and CHU_0153. Thus, both RavA and CHU_0153 appear to have simpler H2-insert motifs compared to BchI.

A third structural difference lies in the oligomeric state of the proteins as deduced from fitting the X-ray structures of the monomers into the EM density maps of the hexamers in the ADP-bound state (El Bakkouri et al., 2010; Lundqvist et al., 2010). While RavA adopts the typical hexameric state with a general sixfold symmetry like many other AAA+ ATPases (Fig 5, top panel), BchI shows a distinct trimer-of-dimers arrangement with a threefold symmetry (Fig. 5, bottom panel). In addition, the orientation of the AAA+ domains is different between the two proteins. For RavA, the back of the AAA+ domain faces the top of the hexamer and tilts away from the central pore, whereas for BchI, the back of the AAA+ domain faces the side of the hexamer with one monomer in each of the

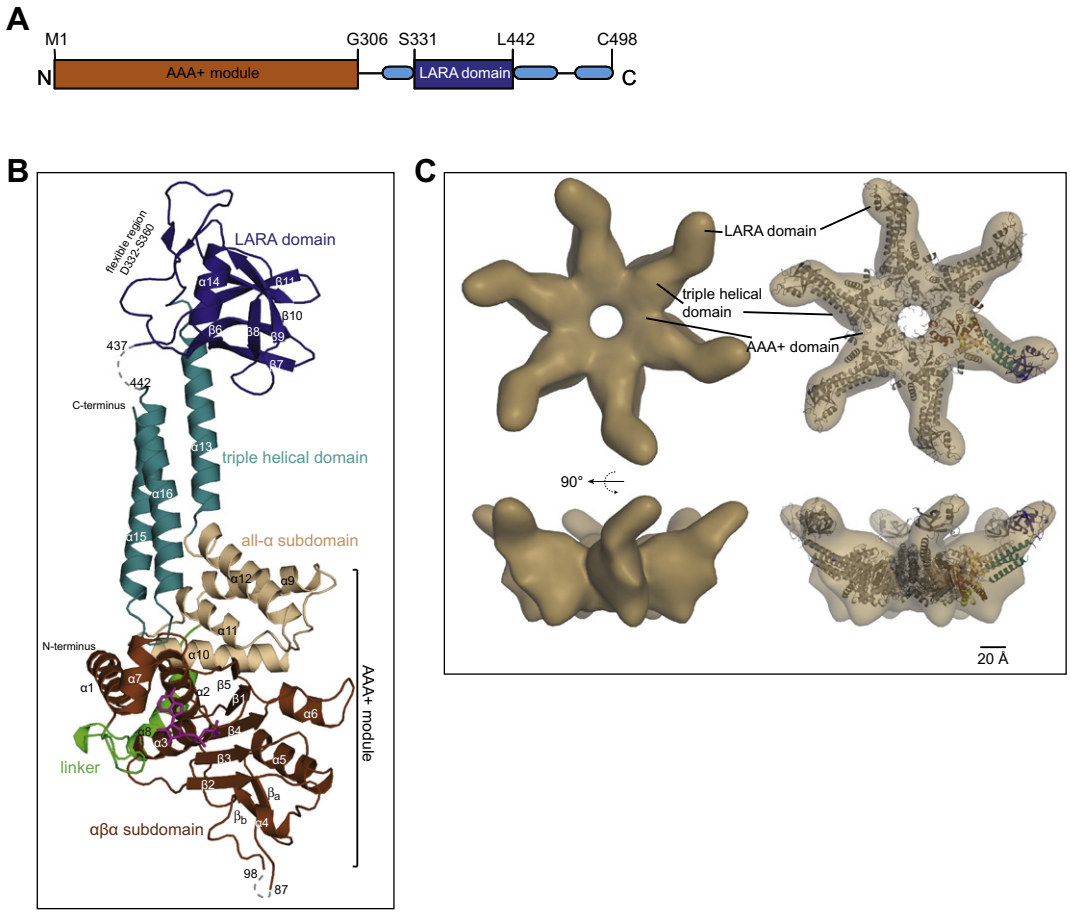

Fig.6. Structure of RavA. (A) A schematic of the RavA domain organization. (B) X-ray structure of RavA protomer. αβα subdomain is shown in brown, all-α subdomain is shown in wheat, the linker between the two subdomains is shown in green, triple helical bundle domain is shown in blue, the LARA domain is shown in dark blue, and bound ADP is shown in violet. The α-helices and β-strands are labeled sequentially except for βa and βb of the Pre-Sensor 1 β-Hairpin insertion. Residues 88–97 and 438–441 were not observed in the X-ray structure and are indicated by a dashed line. (C) Top and side views of the EM 3D reconstruction of the RavA-ADP hexamer. An atomic model of RavA hexamer was generated from the X-ray structure of the RavA protomer by docking into the EM envelope of the hexamer and comparison with the X-ray structure of the HslU hexamer (PDB ID code 1DO0). Figures B and C are from reference (El Bakkouri et al., 2010).

three dimeric subunits tilting at an angle relative to the other monomer (as indicated by their respective helical linker regions, colored in green in Fig. 5, bottom panel). As a result, the RavA hexamer has a more compact central core, while the BchI hexamer shows a large pore in its center (Fig. 5). Hypothetically, the same inherent structural characteristics may be extended to other members of the respective families.

3.3. The structure of the E. coli RavA-LdcI complex

As mentioned earlier, the X-ray crystal structure of the RavA protomer was recently determined by our group (Fig. 6A and B) (El Bakkouri et al., 2010) and shows that the protein has three domains: an N-terminal AAA+ domain and a small, unique, β-rich domain that we named the LARA domain which interacts with LdcI; these domains are separated by a discontinuous triple helical bundle domain. A negative-stain electron-microscopy (EM) reconstruction of the RavA hexamer shows that the protein has a hexameric, flower-like arrangement (Fig. 5, top panel and Fig. 6C) (Snider et al., 2006; El Bakkouri et al., 2010).

LdcI is a 715 amino acids-long (Meng and Bennett, 1992) pyridoxal phosphate (PLP)-dependent decarboxylase (Sabo et al., 1974) that catalyzes the decarboxylation of L-lysine to form the polyamine cadaverine in a reaction that consumes a proton and generates CO_2, which diffuses out of the cell. Cadaverine is removed from the cell by the antiporter CadB, which at the same time imports lysine into the cell. We solved the structure of LdcI (Fig. 7A) and showed that it has three domains: Wing, Core, and C-terminal domain (Alexopoulos et al., 2008; Kanjee et al., 2011). Five LdcI dimers associate to form a decamer with distinct pentameric symmetry (Fig. 7A). In the course of solving the crystal structure of the enzyme, we made the serendipitous finding of the binding of the stringent response alarmone ppGpp at a specific interface between neighboring dimers in the LdcI decamer (Fig. 7A). Hence, there are ten ppGpp molecules per LdcI decamer. This led us to identify a novel regulatory function for ppGpp in controlling LdcI activity during the acid and stringent stress responses. We found that ppGpp dramatically inhibits LdcI activity.

The reconstitution of the RavA-LdcI complex using purified proteins results in a large, cage-like structure in which five RavA hexamers bridge two LdcI decamers as observed by negative stain electron microscopy (EM) (El Bakkouri et al., 2010) (Fig. 7B). We expect such a complex to be highly abundant in the cell under conditions of acid stress and anaerobiosis (Snider et al., 2006; Kanjee et al., 2011). The complex is about 3 MDa and is as big as the ribosome in size. At this stage it is not clear what is the cellular function of this complex. However, biochemical and cell biological studies showed that RavA can prevent the binding of ppGpp to LdcI to allow the enzyme to remain active even in the presence of the alarmone (El Bakkouri et al., 2010). More importantly, the

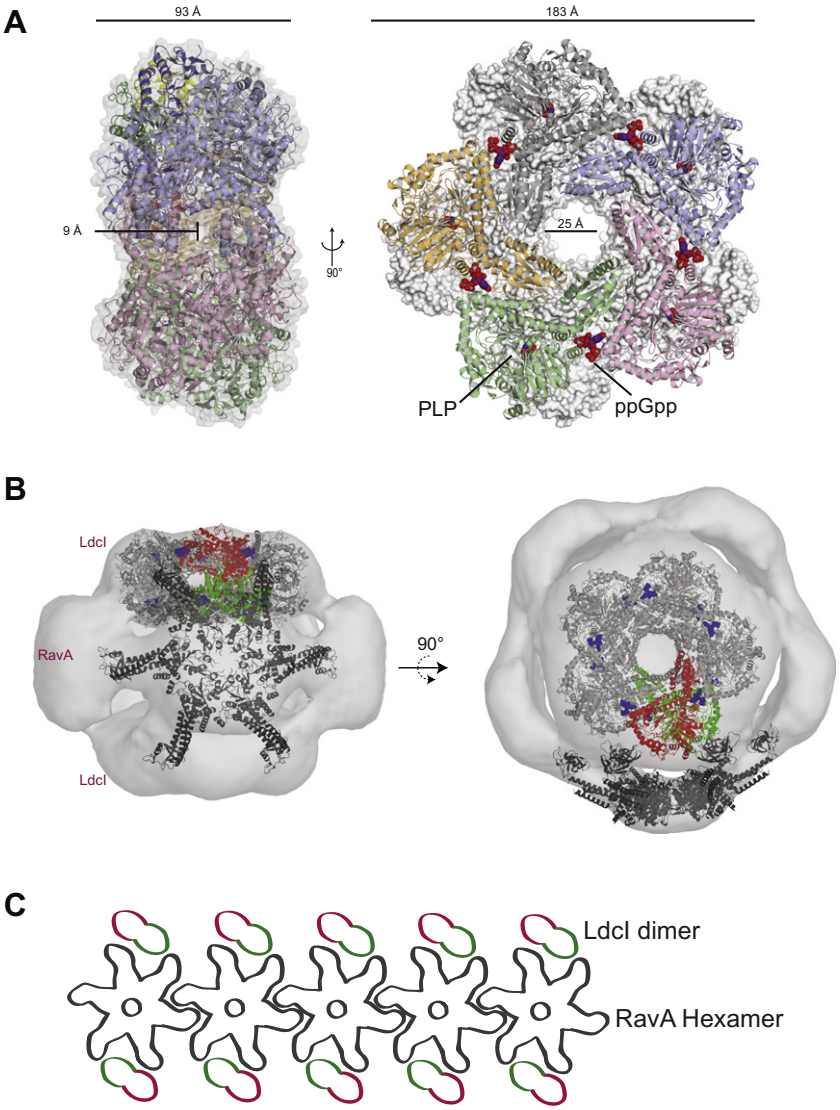

Fig.7. Structure of the RavA-LdcI complex. (A) A cartoon representation of the LdcI decamer is shown beneath a transparent van der Waals' surface. For the structure on the left, neighboring monomers in a dimer are color matched except for those of the top-most pair that are colored according to domains. The dimension of one of the five side pores is indicated. For the structure on the right, The top ring of an LdcI decamer is shown as a cartoon representation, where each monomer has a different color and the bottom ring is shown in gray as a van der Waals' surface. The PLP in each active site and the ppGpp molecules are shown as van der Waals' spheres. Oxygen atoms are in red, nitrogen atoms are in blue, and phosphate atoms are in cyan. The dimension of the central pore is indicated. (B) Fit of the RavA hexameric model and LdcI decamer into the EM envelope of the RavA-LdcI complex viewed from the side (Left) and the top (Right). One LdcI dimer is colored in red (the upper monomer) and green (the lower monomer). ppGpp bound to LdcI is drawn as blue spheres. For clarity, PLP is not shown. (C) A schematic model illustrating RavA-LdcI and RavA–RavA interactions within the RavA-LdcI cage-like structure. Figure A is from reference (Kanjee et al., 2011), while Figures B and C are from reference (El Bakkouri et al., 2010).

LARA domain of RavA seems to bind at a site in LdcI close to the ppGpp binding site and, hence, competes with ppGpp for binding to the decarboxylase. We showed that the LARA domain is required for the RavA-LdcI interaction, as well as, for the RavA-RavA interaction in the RavA-LdcI cage structure (Fig. 7B and C) (El Bakkouri et al., 2010). As shown schematically in Fig. 7C, two legs (triple helical domain + LARA domain) from RavA bind the upper LdcI decamer: one leg binds an LdcI subunit in the upper pentamer and the second leg binds a correponding subunit in the lower pentamer. The interactions seem to be mainly mediated by the LARA domain. The same set of interactions are found with an LdcI dimer at the bottom of the complex. The two remaining legs of RavA are interacting with a neighboring RavA leg on the left and on the right (Fig. 7C). The RavA-RavA leg–leg interactions seem to involve the triple-helical domain, as well as, the LARA domain. Hence, the unique structure of RavA makes all these interactions possible.

4. Closing remarks

The recent structural and functional characterization of known and newly identified MoxR proteins has provided valuable insight into this family of AAA+ ATPases that has remained largely poorly characterized. The majority of the examples discussed here have uncovered previously unknown roles of MoxR proteins in multiple stress response pathways (Table 1). The exact type of stress response associated depends largely on the organisms in which the proteins are found. For example, RL3499 from *R. leguminosarum* is important for stress tolerance in the cell envelope, which in turn is important for establishing optimal symbiosis between the bacterium and the host pea plant (Vanderlinde et al., 2011). FTL_0200 is associated with stress tolerance against the host's immune responses for the pathogenic *F. tularensis* (Dieppedale et al., 2011). RavA is associated with both acid stress tolerance and the stringent response, both of which are experienced during the life cycle of

E. coli (El Bakkouri et al., 2010; Kanjee et al., 2011). An equally intriguing revelation is the link of MoxR proteins to cellular morphology and development, as seen in the requirement of RL3499 for maintaining normal cell morphology in *R. leguminosarum* (Vanderlinde et al., 2011), and the implication of p618 in extracellular viral tail development of the crenarchaeal *Acidianus* two-tailed virus (ATV) (Scheele et al., 2011). Importantly, the functional diversity displayed among MoxR proteins is likely reflected in the nature of their physical interactors. This is supported by the interaction between RavA and the acid stress-associated LdcI in *E. coli* (Snider et al., 2006; El Bakkouri et al., 2010), as well as, the interaction between p618 and the p800 associated with viral tail formation in ATV (Scheele et al., 2011). Thus, the identification and characterization of the physical interactors of MoxR proteins should be considered as equally important in providing a comprehensive view into the nature of MoxR proteins themselves.

From the structural perspective, the X-ray crystal structures of *E. coli* RavA and *C. hutchinsonii* CHU_0153 enable the identification of structural features that are potentially characteristic of the MoxR family proteins. These include: (a) an atypical spatial arrangement of the αβα and all-α subdomains of the AAA+ domain that is also found in the closely related BchI from *R. capsulatus*; (b) the presence of a linker region that, unlike the extended helical structure observed in BchI, takes on a flexible-loop conformation in its N-terminal part and a short helix in the C-terminal part; (c) the presence of an extended α1 helix that occupies the same space as the helical linker region in BchI; (d) a simple structural motif for the helix-2 insert; and (e) a hexameric state resembling the typical configuration of many other AAA + ATPases instead of the trimer-of-dimers configuration of BchI. Nevertheless, to further generalize these structural features requires obtaining more structures of MoxR AAA+ proteins from the different subfamilies.

In conclusion, the detailed functional and structural characterization of other MoxR proteins is necessary to determine the cellular roles and mechanisms of function of this diverse family of AAA+ ATPases.

Acknowledgments

K.S.W. is the recipient of a fellowship from the Canadian Institutes of Health Research (CIHR) Strategic Training Program in Protein Folding and Interaction Dynamics: Principles and Diseases (TGF-53910) and a Doctoral Completion Award from the University of Toronto. This work was supported by a grant from the CIHR to W.A.H. (MOP-67210).

References

Alexopoulos, E., Kanjee, U., Snider, J., Houry, W.A., Pai, E.F., 2008. Crystallization and preliminary X-ray analysis of the inducible lysine decarboxylase from *Escherichia coli*. Acta Crystallogr. Sect. F 64, 700–706.

Aono, R., Sanada, T., 1994. Hyper-autolysis of the faculatative alkaliphile *Bacillus* sp. C-125 cells grown at neutral pH: culture-pH dependent cross-linking of the peptide moieties of the peptidoglycan. Biosci. Biotechnol. Biochem. 58, 2015–2019.

Arai, H., Kodama, T., Igarashi, Y., 1999. Effect of nitrogen oxides on expression of the *nir* and *nor* genes for denitrification in *Pseudomonas aeruginosa*. FEMS Microbiol. Lett. 170, 19–24.

Bartnikas, T.B., Tosques, I.E., Laratta, W.P., Shi, J., Shapleigh, J.P., 1997. Characterization of the nitric oxide reductase-encoding region in *Rhodobacter sphaeroides 2.4.3*. J. Bacteriol. 179, 3534–3540.

Bochtler, M., Hartmann, C., Song, H.K., Bourenkov, G.P., Bartunik, H.D., et al., 2000. The structures of HslU and the ATP-dependent protease HslU-HslV. Nature 403, 800–805.

Cashel, M., Gentry, D.R., Hernandez, V.J., Vinella, D., 1996. The stringent response. In: Curtiss, R., Neidhardt, F.C. (Eds.), *Escherichia coli* and *Salmonella*: Cellular and Molecular Biology. ASM Press, Washington, D.C, pp. 1458–1496.

de Boer, A.P., van der Oost, J., Reijnders, W.N., Westerhoff, H.V., Stouthamer, A.H., et al., 1996. Mutational analysis of the *nor* gene cluster which encodes nitric-oxide reductase from *Paracoccus denitrificans*. Eur. J. Biochem. 242, 592–600.

Dieppedale, J., Sobral, D., Dupuis, M., Dubail, I., Klimentova, J., et al., 2011. Identification of a putative chaperone involved in stress resistance and virulence in *Francisella tularensis*. Infect. Immun. 79, 1428–1439.

Dobbek, H., Gremer, L., Meyer, O., huber, R., 1999. Crystal structure and mechanism of CO dehydrogenase, a molybdo iron–sulphur flavoprotein containing *S*-selanylcysteine. PNAS 96, 8884–8889.

Dominguez, D.C., 2004. Calcium signalling in bacteria. Mol. Microbiol. 54, 291–297.

Edgar, R.C., 2004. MUSCLE: multiple sequence alignment with high accuracy and high throughput. Nucleic Acids Res. 32, 1792–1797.

El Bakkouri, M., Gutsche, I., Kanjee, U., Zhao, B., Yu, M., et al., 2010. Structure of RavA MoxR AAA+ protein reveals the design principles of a molecular cage modulating the inducible lysine decarboxylase activity. PNAS 107, 22499–22504.

Fodje, M.N., Hansson, A., Hansson, M., Olsen, J.G., Gough, S., et al., 2001. Interplay between an AAA module and integrin I domain may regulate the function of magnesium chelatase. J. Mol. Biol. 311, 111–122.

Fuhrmann, S., Ferner, M., Jeffke, T., Henne, A., Gottschalk, G., et al., 2003. Complete nucleotide sequence of the circular megaplasmid pHCG3 of *Oligotropha carboxidovorans*: function in the chemolithoautotrophic utilization of CO, H_2 and CO_2. Gene 322, 67–75.

Hammes, W., Schleifer, K.H., Kandler, O., 1973. Mode of action of glycine on the biosynthesis of peptidoglycan. J. Bacteriol. 116, 1029–1053.

Iyer, L.M., Leipe, D.D., Koonin, E.V., Aravind, L., 2004. Evolutionary history and higher order classification of AAA+ ATPases. J. Struct. Biol. 146, 11–31.

Jungst, A., Zumft, W.G., 1992. Interdependence of respiratory NO reduction and nitrite reduction revealed by mutagenesis of *nirQ*, a novel gene in the denitrification gene cluster of *Pseudomonas stutzeri*. FEBS Lett. 314, 308–314.

Kanjee, U., Gutsche, I., Alexopoulos, E., Zhao, B., El Bakkouri, M., et al., 2011. Linkage between the bacterial acid stress and stringent responses: the structure of the inducible lysine decarboxylase. EMBO J. 30, 931–944.

Li, Z.F., Li, B., Liu, Z.G., Wang, M., Gu, Z.B., et al., 2009. Calcium leads to further increase in glycine-enhanced extracellular secretion of recombinant α-cyclodextrin glycosyltransferase in *Escherichia coli*. J. Agric. Food Chem. 57, 6231–6237.

Lundqvist, J., Elmlund, H., Wulff, R.P., Berglund, L., Elmlund, D., et al., 2010. ATP-induced conformational dynamics in the AAA+ motor unit of magnesium chelatase. Structure 18, 354–365.

Meng, S.Y., Bennett, G.N., 1992. Nucleotide sequence of the *Escherichia coli* cad operon: a system for neutralization of low extracellular pH. J. Bacteriol. 174, 2659–2669.

Meyer, O., Gremer, L., Ferner, R., Ferner, M., Dobbek, H., et al., 2000. The role of Se, Mo and Fe in the structure and function of carbon monoxide dehydrogenase. Biol. Chem. 381, 865–876.

Newton, W.E., 2000. Nitrogen fixation in perspective. In: Pedrosa, F O et al. (Eds.), Nitrogen Fixation: From Molecules to Crop Productivity. Springer, pp. 3–8.

Nystrom, T., 2004. Stationary-phase physiology. Annu. Rev. Microbiol. 58, 161–181.

Oldroyd, G.E.D., Downie, J.A., 2008. Coordinating nodule morphogenesis with *rhizobial* infection in legumes. Ann. Rev. Plant Biol. 59, 519–546.

Pelzmann, A., Ferner, M., Gnida, M., Meyer-Klaucke, W., Maisel, T., et al., 2009. The CoxD protein of *Oligotropha carboxidovorans* is a predicted AAA+ ATPase chaperone involved in the biogenesis of the CO dehydrogenase [$CuSMoO_2$] cluster. J. Biol. Chem. 284, 9578–9586.

Prangishvili, D., Vestergaard, G., Haring, M., Aramayo, R., Basta, T., et al., 2006. Structural and genomic properties of the Hyperthermophilic Archaeal virus ATV with an extracellular stage of the reproductive cycle. J. Mol. Biol. 359, 1203–1216.

Sabo, D.L., Boeker, E.A., Byers, B., Waron, H., Fischer, E.H., 1974. Purification and physical properties of inducible Escherichia coli lysine decarboxylase. Biochemistry (Mosc) 13, 662–670.

Santic, M., Al-khodor, S., Kwaik, Y.A., 2010. Cell biology and molecular ecology of *Francisella tularensis*. Cell. Microbiol. 12, 129–139.

Scheele, U., Erdmann, S., Ungewickell, E.J., Felisberto-Rodrigues, C., Ortiz-Lombardia, M., et al., 2011. Chaperone role for proteins p618 and p892 in the extracellular tail development of *Acidianus* two-tailed virus ATV. J. Virol. 85, 4812–4821.

Snider, J., Thibault, G., Houry, W.A., 2008. The AAA+ superfamily of functionally diverse proteins. Genome Biol. 9, 216.

Snider, J.D., Houry, W.A., 2006. MoxR AAA+ ATPases: a novel family of molecular chaperones? J. Struct. Biol. 156, 200–209.

Snider, J.D., Gutsche, I., Lin, M., Baby, S., Cox, B., et al., 2006. Formation of a distinctive complex between the inducible bacterial lysine decarboxylase and a novel AAA+ ATPase. J. Biol. Chem. 281, 1532–1546.

Springer, T.A., 2006. Complement and the multifaceted functions of VWA and integrin I domains. Structure 14, 11–16.

Tang, Y.P., Dallas, M.M., Malamy, M.H., 1999. Characterization of the BatI (*Bacteroides aerotolerance*) operon in *Bacteroides fragilis*: isolation of a *B. fragilis* mutant with reduced aerotolerance and impaired growth in *in vivo* model systems. Mol. Microbiol. 32, 139–149.

Toyama, H., Anthony, C., Lidstrom, M.E., 1998. Construction of insertion and deletion *mxa* mutants of *Methylobacterium extorquens* AM1 by electroporation. FEMS Microbiol. Lett. 166, 1–7.

Vaara, M., 1992. Agents that increase the permeability of the outer membrane. Microbiol. Rev. 56, 395–411.

van Spanning, R.J., Wansell, C.W., de Boer, T., Hazelaar, M.J., Anazawa, H., et al., 1991. Isolation and characterization of the *moxJ*, *moxG*, *moxI*, and *moxR* genes of

Paracoccus denitrificans: inactivation of *moxJ*, *moxG*, and *moxR* and the resultant effect on methylotrophic growth. J. Bacteriol. 173, 6948–6961.

Vanderlinde, E.M., Magnus, S.A., Tambalo, D.D., Koval, S.F., Yost, C.K., 2011. Mutation of a broadly conserved operon (RL3499-RL3502) from *Rhizobium leguminosarum* biovar viciae causes defects in cell morphology and envelope integrity. J. Bacteriol. 193, 2684–2694.

Wang, J., Song, J.J., Franklin, M.C., Kamtekar, S., Im, Y.J., et al., 2001. Crystal structures of the HslVU peptidase-ATPase complex reveal an ATP-dependent proteolysis mechanism. Structure 9, 177–184.

Whittaker, C.A., Hynes, R.O., 2002. Distribution and evolution of von Willebrand/integrin A domains: widely dispersed domains with roles in cell adhesion and elsewhere. Mol. Biol. Cell 13, 3369–3387.